Click Here for Full Article

Hurricane storm surge simulations comparing three-dimensional with two-dimensional formulations based on an Ivan-like storm over the Tampa Bay, Florida region

Robert H. Weisberg[1] and Lianyuan Zheng[1]

Received 9 September 2008; accepted 6 October 2008; published 4 December 2008.

[1] We provide a dynamics-based comparison on the results from three-dimensional and two-dimensional simulations of hurricane storm surge. We begin with the question, What may have occurred in the Tampa Bay, Florida vicinity had Hurricane Ivan made landfall there instead of at the border between Alabama and Florida? This question is explored using a three-dimensional, primitive equation, finite volume coastal ocean model. The results show that storm surges are potentially disastrous for the Tampa Bay area, especially for landfalls located to the north of the bay mouth. The worst case among the simulations considered is for landfall at Tarpon Springs, such that the maximum wind is positioned at the bay mouth. Along with such regional aspects of storm surge, we then consider the dynamical balances to assess the importance of using a three-dimensional model instead of the usual, vertically integrated, two-dimensional approach to hurricane storm surge simulation. With hurricane storm surge deriving from the vertically integrated pressure gradient force tending to balance the difference between the surface and bottom stresses, we show that three-dimensional structure is intrinsically important. Two-dimensional models may overestimate (or underestimate) bottom stress, necessitating physically unrealistic parameterizations of surface stress or other techniques for model calibration. Our examination of the dynamical balances inherent to storm surges over complex coastal topography suggests that three-dimensional models are preferable over two-dimensional models for simulating storm surges.

Citation: Weisberg, R. H., and L. Zheng (2008), Hurricane storm surge simulations comparing three-dimensional with two-dimensional formulations based on an Ivan-like storm over the Tampa Bay, Florida region, *J. Geophys. Res.*, *113*, C12001, doi:10.1029/2008JC005115.

1. Introduction

[2] Hurricane Ivan, attaining Saffir-Simpson scale category 5 status in the Caribbean Sea on 12 September 2004, entered the Gulf of Mexico (GOM) and weakened to a category 4 hurricane on 14 September 2004. It then weakened further before making landfall at the border between Alabama and Florida (Figure 1) as a category 3 hurricane on 16 September 2004. Hurricane Ivan produced storm surges of about 3.6 m along Pensacola Beach and 4.5 m within Pensacola Bay [*Hagy et al.*, 2006]. Coupled with large waves [*Wang et al.*, 2005], Ivan caused extensive damage to coastal and inland structures, highways and bridge systems, and forests [*Hagy et al.*, 2006; *Sallenger et al.*, 2006], making it one of the most destructive hurricanes to ever hit the Pensacola Bay area. If a hurricane of similar magnitude were to make landfall near the more densely populated Tampa Bay area (Figure 2), what might the potential for inundation by storm surge be? This is the question that motivated our study.

[1]College of Marine Science, University of South Florida, St. Petersburg, Florida, USA.

Copyright 2008 by the American Geophysical Union.
0148-0227/08/2008JC005115$09.00

[3] The vulnerability of the Tampa Bay region to inundation by hurricane storm surge increases each year with added coastal development. Whereas direct, major hurricane hits occurred on only two occasions: 1848, when there was virtually no development and 1921, when there was only nominal development, the occurrence of two successively active years with Charley, Frances, Ivan, and Jeanne in 2004 followed by Dennis, Katrina, Rita, and Wilma in 2005 have heightened concerns. Moreover, the broad, gently sloping nature of the West Florida Continental Shelf [e.g., *Weisberg et al.*, 2005] combined with the shallowness and length of Tampa Bay [e.g., *Weisberg and Zheng*, 2006a] and the low elevations [e.g., *Weisberg and Zheng*, 2006b] are all conducive to large storm surge [*Signorini et al.*, 1992], suggesting that increased public awareness is necessary to protect life and property.

[4] The life and property risks place coastal inundation by hurricane storm in the purview of government agencies. NOAA is generally recognized as providing advisories through the National Weather Service, FEMA underwrites the Federal Flood Insurance Program, and local emergency management offices coordinate local affairs. Hurricane storm surge models are therefore commonplace, and simulations are available for most coastal regions, Tampa Bay included. However, all models have their limitations, as do

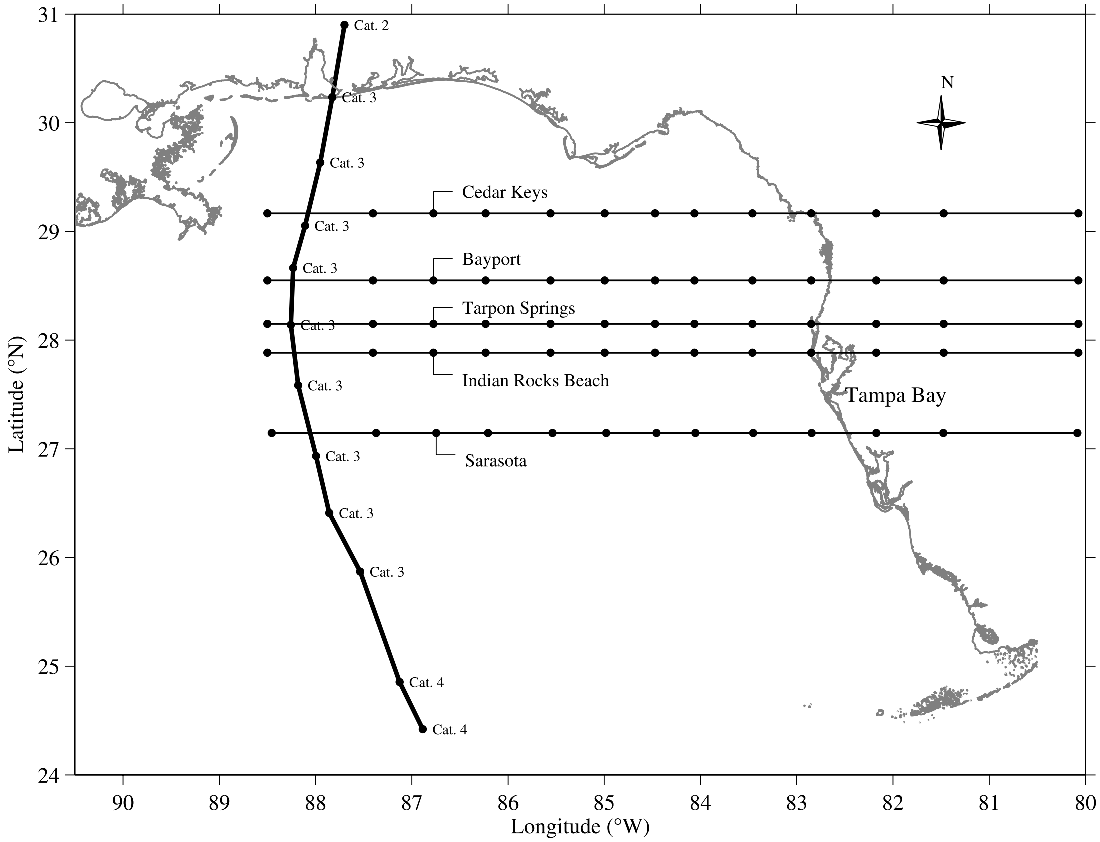

Figure 1. The Hurricane Ivan track line and its Saffir-Simpson scale category approaching the Florida/Alabama border along with the five rotated track lines used in this study. From south to north, these are designated by their points of landfall: Sarasota (SA), Indian Rocks Beach (IRB), Tarpon Springs (TS), Bayport (BP), and Cedar Keys (CK). The dots indicate the locations where the H*Wind data as augmented by the prototypical hurricane data of *Holland* [1980] are applied.

the methods of information dissemination. Hence we engaged in two descriptive studies [*Weisberg and Zheng*, 2006b, 2006c], the first exploring storm surge sensitivities to storm structure, intensity, direction and speed of approach, and point of landfall and the second being an actual simulation for Hurricane Charley to improve public awareness of the inundation potential by hurricane storm surge for the west coast of Florida. We expand on these previous studies here by considering an actual storm scenario; that of Hurricane Ivan, but with the track diverted to Tampa Bay.

[5] Along with describing the inundation potential, we also consider the dynamical balances associated with the storm surge evolution and, in particular, the differences that may arise when applying three-dimensional (3-D) versus two-dimensional (2-D) models. The importance of this study stems from the fact that the models routinely in use by agencies are 2-D (e.g., SLOSH by NOAA [e.g., *Jelesnianski et al.*, 1992] and ADCIRC by FEMA and the USACE [e.g., J. J. Westerink et al., A basin to channel scale unstructured grid hurricane storm surge model as implemented for southern Louisiana, submitted to *Monthly Weather Review*, 2008, hereinafter referred to as Westerink et al., submitted manuscript, 2008]). The question of 2-D versus 3-D modeling follows from the force balances that give rise storm surge. Storm surge derives from the tendency of vertically integrated pressure gradient force (due to the sea surface slope) to balance the difference between the surface and bottom stresses. The surface stress is the wind stress. The bottom stress is where 2-D and 3-D models differ. In either case bottom stress usually follows a quadratic friction law, but in the 2-D case this is based on depth-averaged velocity, whereas in the 3-D case it is based on the near-bottom velocity. So the bottom stress will differ in these two formulations to the extent that the near-bottom velocity differs from the vertically averaged velocity, and this affects the surge estimation.

[6] The paper is organized as follows. Section 2 introduces the model and the experiments performed. Section 3 describes the results of the Ivan-like hurricane with landfall in the Tampa Bay vicinity. Section 4 explores the dynamical balances associated with the storm surge and compares those obtained with either 2-D or 3-D formulations. Section 5 discusses the parameters used for calculating the wind and bottom stresses and their effects on the estimated storm surges. A summary and a set of conclusions are given in section 6.

2. Model Description and Configuration

2.1. Storm Surge Model

[7] We use the time-dependent, three-dimensional, primitive-equation, finite-volume coastal ocean model (FVCOM) of *Chen et al.* [2003] as modified by *Weisberg and Zheng* [2006b] for the addition of atmospheric pressure gradient

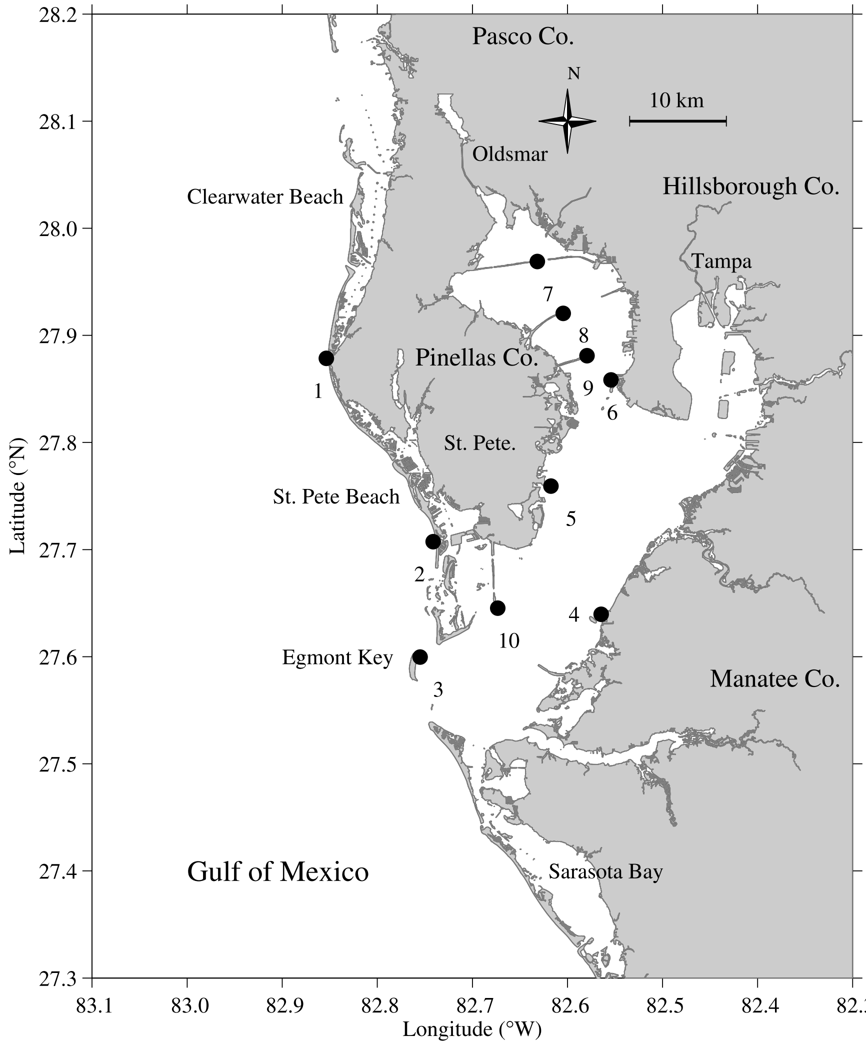

Figure 2. Tampa Bay and the adjacent West Florida Shelf. Solid circles denote locations discussed in the text.

effects. To close the governing momentum and continuity equations by parameterizing the flow-dependent mixing coefficients, FVCOM incorporates the level $2\frac{1}{2}$ turbulence closure submodel of *Mellor and Yamada* [1982], as modified by *Galperin et al.* [1988], for vertical mixing and the formulation for horizontal mixing of *Smagorinsky* [1963]. A terrain-following σ-coordinate transformation in the vertical accommodates irregular bottom topography, and a non-overlapping, unstructured triangular grid in the horizontal fits complex coastlines, headlands, and other structures. FVCOM solves the primitive and turbulence equations using a second-order accurate flux calculation integrated over each model grid control volume. This ensures mass, momentum, energy, salt, and heat conservation in the individual control volumes and also over the entire computational domain [*Chen et al.*, 2003]. Similar to the Princeton Ocean Model (POM) of *Blumberg and Mellor* [1987], a mode-splitting method, with external and internal mode time steps to accommodate the faster and slower barotropic and baroclinic responses, respectively, is used for computational efficiency. FVCOM also includes provision for flooding and drying, a critical element of storm surge simulation [*Hubbert and McInnes*, 1999; *Peng et al.*, 2006; *Weisberg and Zheng*, 2006b, 2006c]. Details of the flooding/drying treatment are provided by *Chen et al.* [2008].

[8] With Boussinesq and hydrostatic approximations, the primitive-equations for momentum and mass conservation are:

$$\frac{\partial(\mathrm{Du})}{\partial t}+\frac{\partial\left(\mathrm{Du}^2\right)}{\partial x}+\frac{\partial(\mathrm{Duv})}{\partial y}+\frac{\partial(\mathrm{u}\omega)}{\partial\sigma}-f\mathrm{Dv} = -\mathrm{gD}\frac{\partial(\eta-\eta_a)}{\partial x}-\frac{\mathrm{gD}^2}{\rho_0}\int_\sigma^0\left[\frac{\partial\rho}{\partial x}-\frac{\sigma}{\mathrm{D}}\frac{\partial \mathrm{D}}{\partial x}\frac{\partial\rho}{\partial\sigma}\right]\cdot d\sigma+\frac{\partial}{\partial\sigma}\left[\frac{\mathrm{K_m}}{\mathrm{D}}\frac{\partial \mathrm{u}}{\partial\sigma}\right]+\mathrm{F_u} \quad (1)$$

$$\frac{\partial(\mathrm{Dv})}{\partial t}+\frac{\partial(\mathrm{Duv})}{\partial x}+\frac{\partial\left(\mathrm{Dv}^2\right)}{\partial y}+\frac{\partial(\mathrm{v}\omega)}{\partial\sigma}+f\mathrm{Du} = -\mathrm{gD}\frac{\partial(\eta-\eta_a)}{\partial y}-\frac{\mathrm{gD}^2}{\rho_0}\int_\sigma^0\left[\frac{\partial\rho}{\partial y}-\frac{\sigma}{\mathrm{D}}\frac{\partial \mathrm{D}}{\partial y}\frac{\partial\rho}{\partial\sigma}\right]\cdot d\sigma+\frac{\partial}{\partial\sigma}\left[\frac{\mathrm{K_m}}{\mathrm{D}}\frac{\partial \mathrm{v}}{\partial\sigma}\right]+\mathrm{F_v} \quad (2)$$

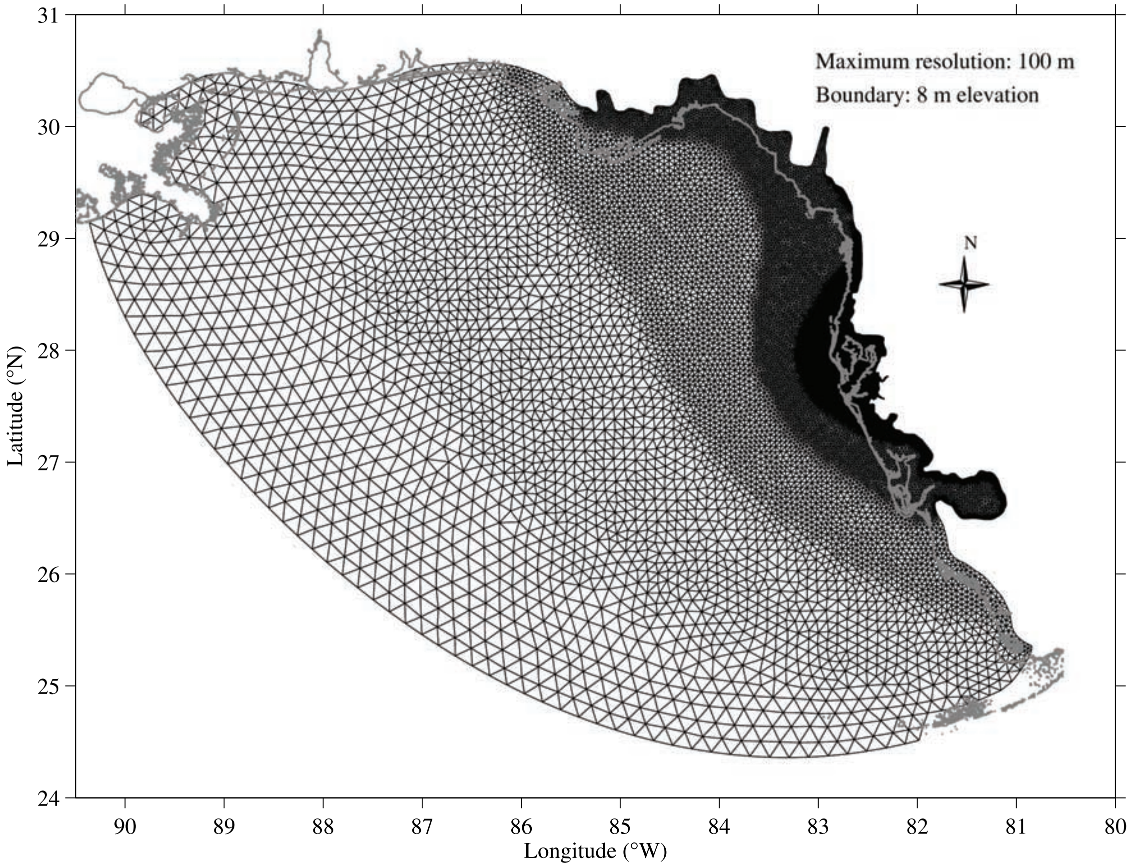

Figure 3a. The unstructured triangular grid used in this study. Model resolution varies from 20 km along the open boundary to 100 m in Pinellas County Intracoastal Waterway and the Pinellas County barrier islands. The model domain extends upland to the 8 m (above mean sea level) elevation contour.

$$\frac{\partial \eta}{\partial \mathrm{t}} + \frac{\partial(\mathrm{Du})}{\partial \mathrm{x}} + \frac{\partial(\mathrm{Dv})}{\partial \mathrm{y}} + \frac{\partial \omega}{\partial \sigma} = 0, \tag{3}$$

where u, v, and ω are the x, y, and σ velocity components; f the Coriolis parameter; g the gravitational acceleration; K_m the vertical eddy viscosity; ρ_0 the reference density; ρ the perturbation density; D = h + η the total water depth, where η and h are the surface elevation and reference depth below the mean sea level, respectively; η_a the sea level displacement induced by the atmospheric pressure perturbation's inverted barometer effect; and F_u and F_v are the horizontal momentum diffusion terms.

[9] The surface and bottom boundary conditions for momentum are

$$\frac{\rho_0 \mathrm{K_m}}{\mathrm{D}}\left(\frac{\partial \mathrm{u}}{\partial \sigma}, \frac{\partial \mathrm{v}}{\partial \sigma}\right) = \left(\tau_{\mathrm{sx}}, \tau_{\mathrm{sy}}\right) \text{ and } \omega = 0, \text{ at } \sigma = 0 \tag{4}$$

$$\frac{\rho_0 \mathrm{K_m}}{\mathrm{D}}\left(\frac{\partial \mathrm{u}}{\partial \sigma}, \frac{\partial \mathrm{v}}{\partial \sigma}\right) = \left(\tau_{\mathrm{bx}}, \tau_{\mathrm{by}}\right) \text{ and } \omega = 0, \text{ at } \sigma = -1, \tag{5}$$

where (τ_{sx}, τ_{sy}) and (τ_{bx}, τ_{by}) are wind stress and bottom stress components, respectively.

[10] At the open boundary, sea surface elevation is calculated by applying a radiation boundary condition using a gravity wave propagation speed, $\sqrt{gh}$. The horizontal velocity components, evaluated at the grid cell centers, are calculated directly from equations (1) and (2) without inclusion of the advection and the vertical and horizontal diffusion terms. At the lateral boundary, no flow normal to solid boundaries is used.

[11] Wind stress is computed by:

$$\vec{\tau}_{\mathrm{s}} = \mathrm{C_d} \rho_{\mathrm{a}} \left|\vec{\mathrm{V}}_{\mathrm{w}}\right| \vec{\mathrm{V}}_{\mathrm{w}}, \tag{6}$$

where ρ_a is air density, $\vec{V}_w$ is wind speed at 10 m height, and C_d, a drag coefficient dependent on wind speed, is given by the *Large and Pond* [1981] formula of :

$$\mathrm{C_d} \times 10^3 = \begin{cases} 1.2 & \left|\vec{\mathrm{V}}_{\mathrm{w}}\right| \geq 11.0\,\mathrm{ms^{-1}} \\ 0.49 + 0.065\left|\vec{\mathrm{V}}_{\mathrm{w}}\right| & 11.0\,\mathrm{ms^{-1}} \leq \left|\vec{\mathrm{V}}_{\mathrm{w}}\right| \leq 25.0\,\mathrm{ms^{-1}} \\ 0.49 + 0.065 \times 25 & \left|\vec{\mathrm{V}}_{\mathrm{w}}\right| \geq 25.0\,\mathrm{ms^{-1}} \end{cases} \tag{7}$$

[12] Bottom stress is determined by:

$$\vec{\tau}_{\mathrm{b}} = \mathrm{C_z} \rho_{\mathrm{w}} \left|\vec{\mathrm{V}}_{\mathrm{b}}\right| \vec{\mathrm{V}}_{\mathrm{b}}, \tag{8}$$

where ρ_w is water density, $\vec{V}_b$ is near-bottom water velocity, and C_z is a bottom drag coefficient determined by matching

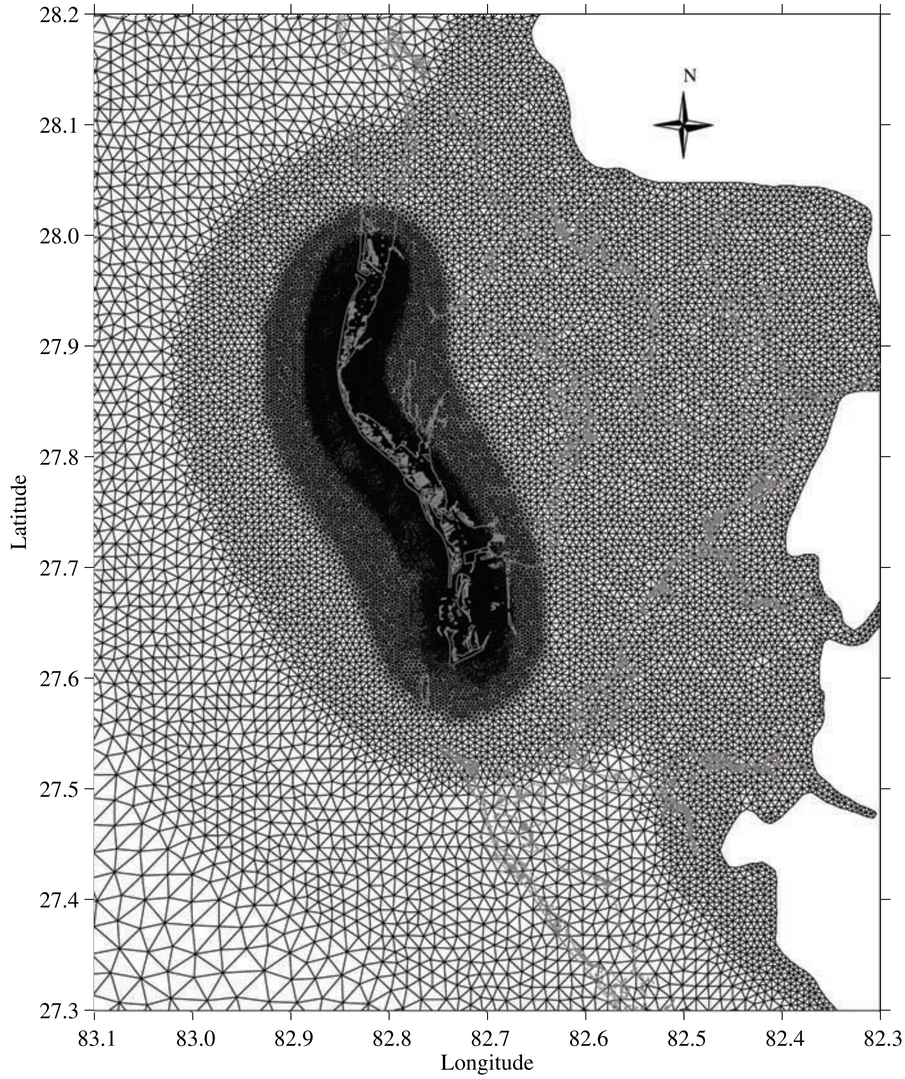

Figure 3b. A zoomed view of the model grid focusing on the Pinellas County Intracoastal Waterway and the Pinellas County barrier islands.

a logarithmic bottom layer to the model at a height of the first σ level above the bottom, i.e.

$$C_z = \max\left\{\frac{k^2}{\left[\ln(1+\sigma_{kb-1})H/z_0\right]^2}, 0.0025\right\} \qquad (9)$$

where k = 0.4 is the von Karman constant, z_0 is bottom roughness parameter, and σ_{kb-1} is the vertical level next to the bottom.

2.2. Model Configuration

[13] Storm surge derives from wind stress and atmospheric pressure forcing, and it is influenced by continental shelf geometry and bathymetry. Whereas storm surge is manifested locally, storm surge simulation must use a domain that is large enough both to contain the meteorological forcing fields and to account for remote effects through coastally trapped wave propagation.

[14] Thus the model domain extends from the Mississippi River delta in the north to the Florida Keys in the south, with an open boundary arching in between (Figure 3a). The grid resolution increases from the open boundary toward the West Florida coast, with the highest resolution (at about 100 m) centered on the Pinellas County Intracoastal Waterway (PCIW) and barrier islands to resolve the inlets and bayous (Figure 3b). The resolution remains less than 300 m throughout Tampa Bay to resolve all of the bridge causeways, and it then diminishes to about 20 km along the open boundary. Once on land, the model domain extends to the 8 m (above mean sea level) elevation contour. This coastal ocean to upland transition allows us to include a flooding/drying algorithm [*Chen et al.*, 2008], with a flooding threshold depth of 10 cm.

[15] Within the model domain there are a total of 88,400 triangular elements, with 44,713 nodes in the horizontal plane and 11 uniformly distributed σ-coordinate levels in the vertical direction. The model grid is superimposed on a joint NOAA/USGS bathymetric/topographic data set with 30 m resolution in the Tampa Bay vicinity [*Hess*, 2001]. Given that most of the populated regions have seawalls and these seawalls are at a nominal height of 1.2 m above mean

sea level, we set the minimum land elevation at 1.2 m, which means that a minimum 1.3 m surge (the sum of the seawall height and threshold value) is required to initiate flooding in the model.

[16] On the basis of Courant-Friedrichs-Levy (CFL) numerical stability condition, computational time steps of 1 s and 10 s are used for the external and internal modes, respectively. Temperature and salinity are specified to be constant at 20°C and 35 PSU, respectively. Excluded from the model simulations are the effects of tides, rivers, density changes (steric), and waves. These all occur in nature, and their effects would be additive to what we present on the basis of winds and atmospheric pressure alone. For instance, steric sea level variations amount to about plus or minus 20 cm (maximum and minimum in late summer and winter, respectively), Tampa Bay tides have a range of about 1 m, and river effects on sea level are generally about 10 cm [e.g., *Weisberg and Zheng*, 2006a]. Wave effects by radiation stress and run-up can add similar values, and, more importantly, the forces by waves on structures can be more destructive than the rising surge waters. Wave effects are beyond the scope of the present investigation, however.

[17] To investigate the storm surge potential for the Tampa Bay area on the basis of an Ivan-like hurricane, we rotated and stretched the actual track from its approximate north-south orientation to exactly east-west (Figure 1), and we further rotated the winds relative to the track. Five such tracks are considered, with landfalls near Sarasota (SA), Indian Rocks Beach (IRB), Tarpon Springs (TS), Bayport (BP), and Cedar Keys (CK). The distances from these landfall points to the Tampa Bay mouth are 30km (SA), 50 km (IRB), 80 km (TS), 125km (BP), and 200 km (CK), respectively.

2.3. External Forcing

[18] External forcing is based on the H*Wind, central atmospheric pressure, maximum wind speed, and radius to maximum winds for Hurricane Ivan downloaded from the National Oceanic and Atmospheric Administration (NOAA), National Hurricane Center (NHC) Web site. These data are available at either 3 hr or 6 hr intervals after Hurricane Ivan entered the Gulf of Mexico (Figure 1). Because our model domain is larger than the post-storm, H*Wind analysis domain, which covers 960 km × 960 km centered on hurricane eye, the model wind was constructed by combining the properly rotated H*Wind (which is asymmetric) with the prototypical hurricane wind field (which is symmetric) of *Holland* [1980]. Given the structural differences between the H*Wind and prototypical wind, we combined the two fields using a linear weighting function. The weighting is such that the wind is purely H*Wind for the inner-most 880 km × 880 km domain centered on the hurricane eye, purely Holland wind for the domain beyond the H*Wind, and a weighted average of the H*Wind and Holland wind over the outer-most 40 km of the H*Wind field. This weighting produces a smooth transition from one wind field to the other. Examples of the model-input wind fields, when the hurricane is located either over the deep-ocean or at the IRB point of landfall, are shown in Figure 4. These examples demonstrate that the combined and rotated model-input wind fields properly represent the H*Wind relative to the new tracks.

[19] The atmospheric pressure fields are calculated using the formulation of *Holland* [1980]:

$$P = P_c + (P_n - P_c)\exp\left(-A/r^B\right) \tag{10}$$

where r is the radial distance from the hurricane center; P is the atmospheric pressure as functions of r; P_n and P_c are the ambient atmospheric pressure and hurricane central atmospheric pressure, respectively; and A and B are storm-scale parameters related via $A = (R_{max})^B$, where R_{max} is the radius of maximum winds.

3. Storm Surge Simulation Results

[20] Of the five tracks, we begin by considering the simulation for the IRB landfall. The results, sampled at four different times, are organized as sets of three panels each in Figures 5a and 5b. The left hand and middle panels are snapshots of the model-simulated storm surge elevation (EL) relative to mean seal level (MSL) and relative to the local land elevation (LE), respectively, and the right hand panels are the model-input wind vectors superimposed on color-coded wind speed contours. The sampling times are at hrs 27, 30, 31, and 32 after the simulation initiation. The asterisks denote the IRB landfall location, and the solid circles denote the storm center. These panels show the surge evolution as the hurricane transits eastward from the deep Gulf of Mexico (at hr 27) to across Tampa Bay (at hr 32). While not shown, we note that in the far field at earlier times there is a sea level rise at the storm center due to the low atmospheric pressure there, i.e., by the inverted barometer effect. By hr 27 (3 hours before landfall), the storm center is located about 60 km west of IRB, the winds in the vicinity of Tampa Bay (Figure 5a, upper panels) are southerly and directed along shore. The wind speeds in this panel vary from 50 ms^{-1} 20 km west of bay mouth to 35 ms^{-1} within the bay. The surge at this time is by a combination of onshore Ekman transport by the downwelling-favorable winds over the shelf, plus a directly forced downwind set up in shallow water. Thus the surge along the St. Pete Beach (SPB) coast is about 3.5 m, causing the SPB region to be inundated by more than 0.5 m water (upper center panel). Within the bayous north of the PCIW, the surge exceeds 5 m, resulting in a flow of water from the PCIW toward Old Tampa Bay. Such bayou flooding eventually leads to the City of St. Petersburg becoming an island. The surge along the Sarasota coast is also substantial, at about 4 m. Inside Tampa Bay, the surge varies from about 2 m at the mouth of the Manatee River (southeast side of the bay where the wind is offshore), to 3.5 m at the upper portion of Hillsborough Bay, to a maximum of 4.5 m at the head of Old Tampa Bay. A general theme of increasing surge magnitude with distance up the bay emerges. This results in large-scale flooding, not only in residential areas, but also in other important locales such as the Tampa International Airport and the McDill Air Force Base (AFB).

[21] The situation degrades significantly at the time of landfall (hr 30). With the winds now directed onshore south of the hurricane center and generally up the bay, the direct effect of these winds piling water up against a windward shoreline in shallow water is dramatic (Figure 5a). Thus,

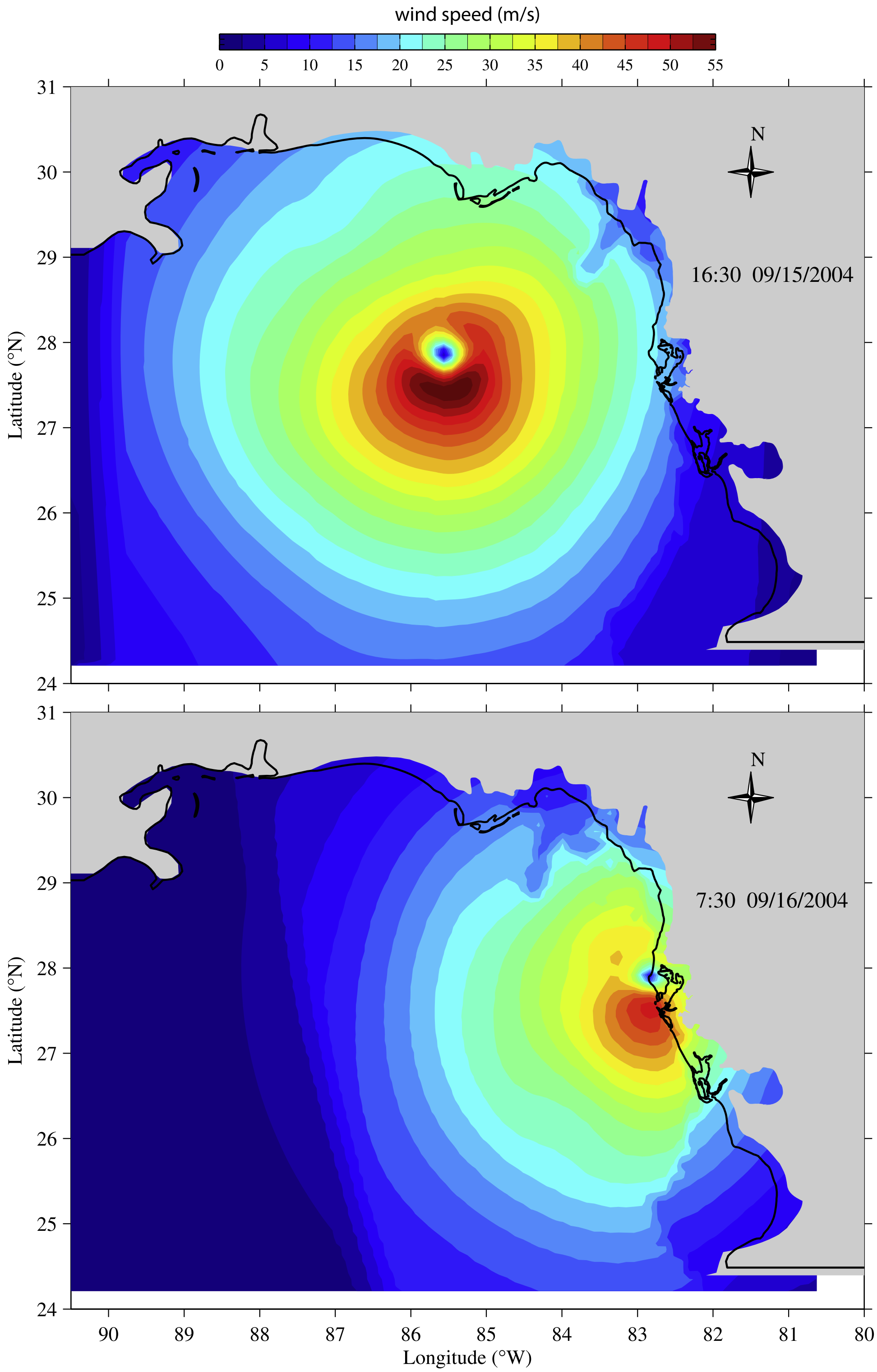

Figure 4. The model-input wind fields sampled 13 hours (top) before IRB landfall and (bottom) at the time of IRB landfall.

with maximum winds of 55 ms^{-1} occurring at the bay mouth and directed almost parallel to the estuary axis, the surge begins at about 3.5 m along the SPB and Sarasota coastlines and increases up the bay, reaching values of 4.5 m in Hillsborough Bay and 5.5 m in Old Tampa Bay. With the water level now higher in Old Tampa Bay than in the PCIW not only does the islanding of St. Petersburg increase, the flow direction reverses to be from the bay to the PCIW. Inundation over large residential tracts is now severe. For instance, northeast St. Petersburg has up to 3 m of water above the land level, and smaller sections around the bay periphery are similarly impacted. In contrast, to the north of

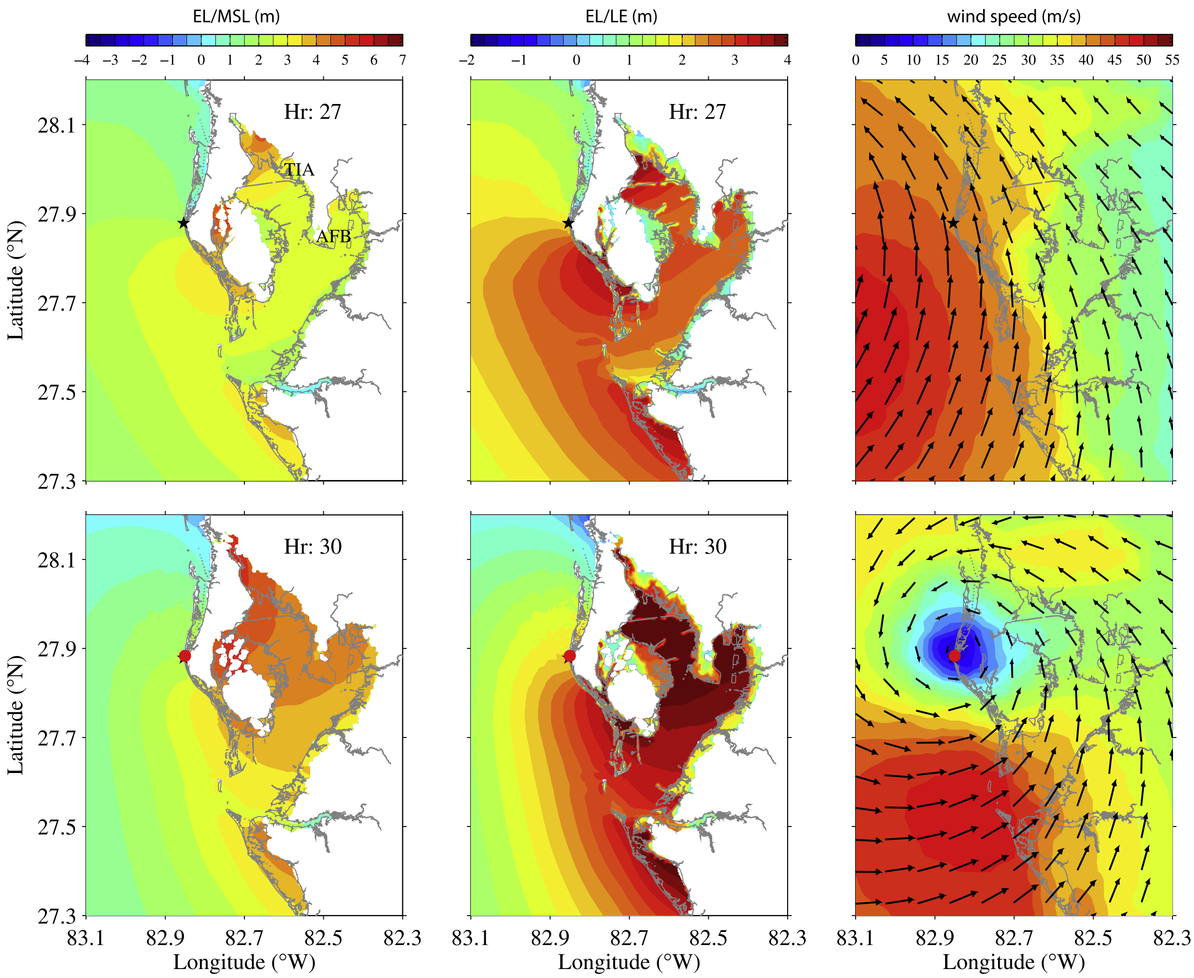

Figure 5a. Planar views of model-simulated surge relative to mean sea level (EL/MSL, left panels), relative to the local land elevations (EL/LE, middle panels), and the wind vectors superimposed on wind speed contours at hours 27 (upper panels) and 30 (lower panels). Hour 30 is the time of IRB landfall. The asterisk denotes the IRB landfall location, and the solid red circle denotes the storm center location.

the hurricane center, such as at Clearwater Beach and at locations farther north, sea level sets down because of offshore winds.

[22] Owing to complex geometry, the time of landfall does not necessarily herald the worst of the storm surge. By hr 31, when the storm center has crossed over the bay, the bay has received its maximum volume of water (Figure 5b). With highest surge values on the Tampa Bay side of Tarpon Springs and lowest values on the Gulf of Mexico side, we see that a flow of water may occur there, connecting the bay with the gulf. It is conceivable then that not only could the bridges linking Pinellas County with the mainland be disrupted or destroyed, the land link between Pinellas and Pasco Counties, also connected by a bridge over the Anclote River, could also be disrupted. In such event Pinellas County could become isolated without any remaining lines of communication after the storm passed. Moreover, with a maximum water volume in the bay and with the winds now changing direction over this water volume, a redistribution occurs that further inundates certain regions, the heavily populated northeast St. Petersburg, in particular. In contrast surge levels are beginning to abate along the Pinellas County gulf beaches.

[23] By hr 32, the hurricane center is positioned about 60 km east of Tampa Bay (Figure 5b). At this time the wind field no longer contains the H*Wind; instead it is constructed entirely by the prototypical hurricane wind field of *Holland* [1980]. Nevertheless it is important to note that even with the storm now distant from Tampa Bay, the reversal in wind direction on the tail end of the storm causes the water that had piled up in the bay to redistribute toward the eastern shore, resulting in maximum inundation to residential areas situated there. Thus inundation exceeding 4 m above the land elevation occurs at Apollo Beach. Similarly, the Manatee River (located at the southeast corner of the bay) shows substantial inundation to adjacent residential neighborhoods by as much as 4 m above the land elevation.

[24] The primary lesson of Figures 5a and 5b is that the surge evolution entails a complex interaction between meteorological forcing and local geometry. It is for this reason that a model with complete-enough physics, high-enough horizontal resolution, and provision for flooding

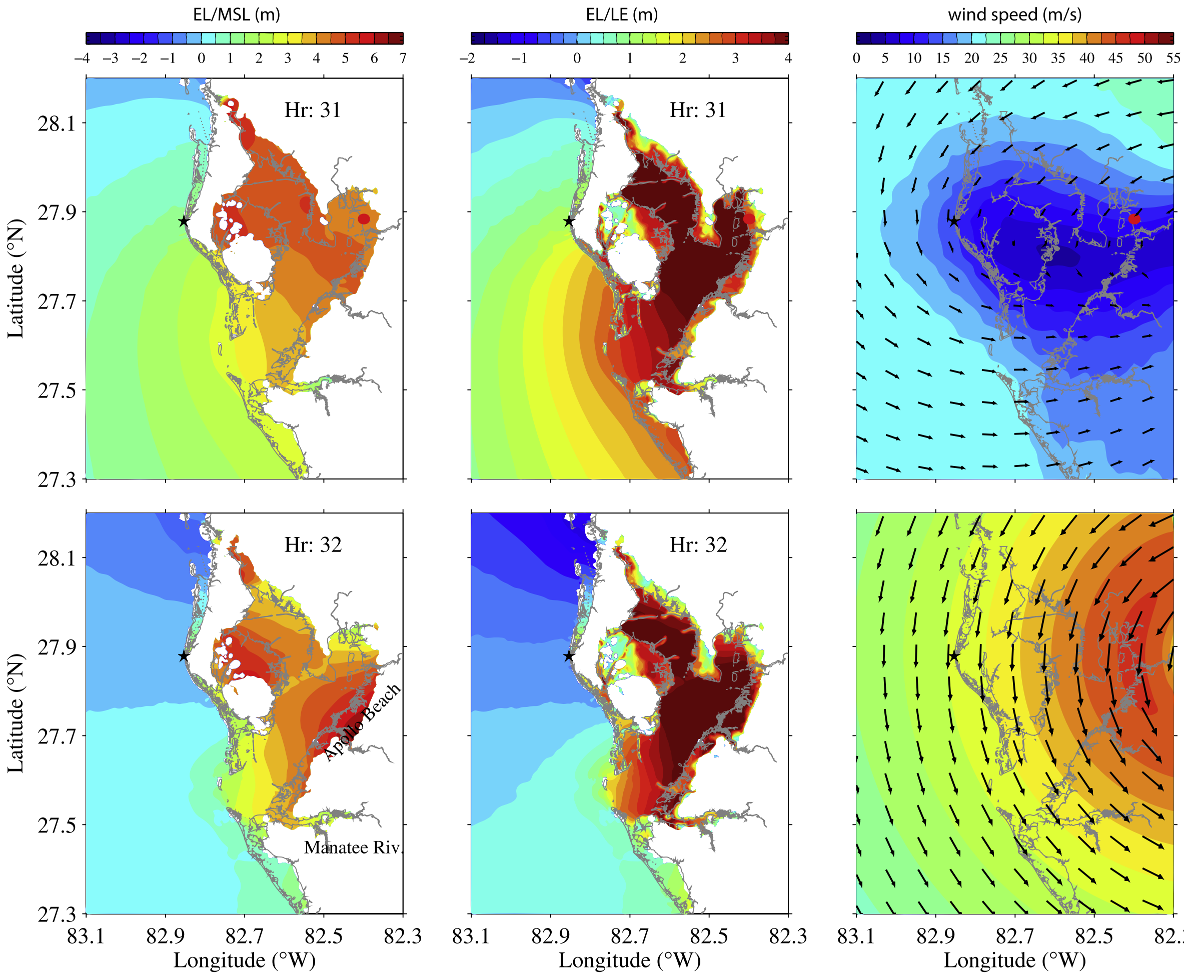

Figure 5b. Same as Figure 5a except for sampling at hours 31 (upper panels) and 32 (lower panels).

and drying is necessary for storm surge simulation. To provide a better sense of the spatial complexities of the surge response, Figure 6 shows the worst flooding scenarios for different sections of the model domain, as occurs at certain specific times. In all of the panels the surge level is given relative to the local land elevation. We see that the Pinellas County beaches can be inundated by as much as 2.5 m, northeast St. Petersburg by as much as 4.5 m, Tampa International Airport and McDill AFB by 3 m, Davis Islands and Tampa General Hospital by 2.5 m, and Apollo Beach by up to 5 m. The potential for catastrophic damage is obvious, not only to residences, but also to critical infrastructure.

[25] Time series of the model-simulated surge sampled at some critical locations are presented in Figure 7. Counterclockwise from the top left we consider the beach communities of IRB and SPB, the mouth of the bay at Egmont Key (EK), the commercial area of Port Manatee (PM), downtown St. Petersburg (SP), and the commercial area of Port of Tampa (PT), followed by the four major bridge causeways linking Pinellas County with Hillsborough and Manatee Counties, the Courtney Campbell Causeway (CCC), the Howard Frankland Bridge (HFB), the Gandy Bridge (GB), and the Sunshine Skyway Bridge (SSB), the locations of which are shown in Figure 2. Sea level begins to rise at the gulf coast locations (IRB, SPB, and EK) by hr 7, as a result of Ekman transport, which is the precursor of the storm surge. The rate of rise of sea level increases as the winds increase and as local downwind set-up comes into play (by the tendency for the pressure gradient force to balance the difference between the surface and bottom stresses). While the storm surge varies primarily with the winds, both the time of peak surge and the phase relative to the winds is a matter of local geometry making generalizations difficult.

[26] Figure 7 also compares the results for the various points of landfall that are considered. Beginning with the Sarasota landfall, we see that the surge values at the sampled locations tend to be minimal since, with the storm center being south of the bay mouth, the wind is directed offshore for the most part. Nevertheless there are some regions that experience a set up for reasons of local shoreline orientation relative to the winds at any given point in the storm progression. Next consider the comparison between the IRB and the TS landfalls. These are generally very similar, but with the TS landfall providing slightly higher inundation at the bridge causeways located in Old Tampa Bay. This is because the TS landfall places the maximum winds for this Ivan-like storm right at the Tampa Bay mouth. The storm surge then decreases as the point of landfall moves farther north to BP and CK. However, even though CK is located some 200 km north of the Tampa Bay mouth, a surge of about half the magnitude of the TS or IRB

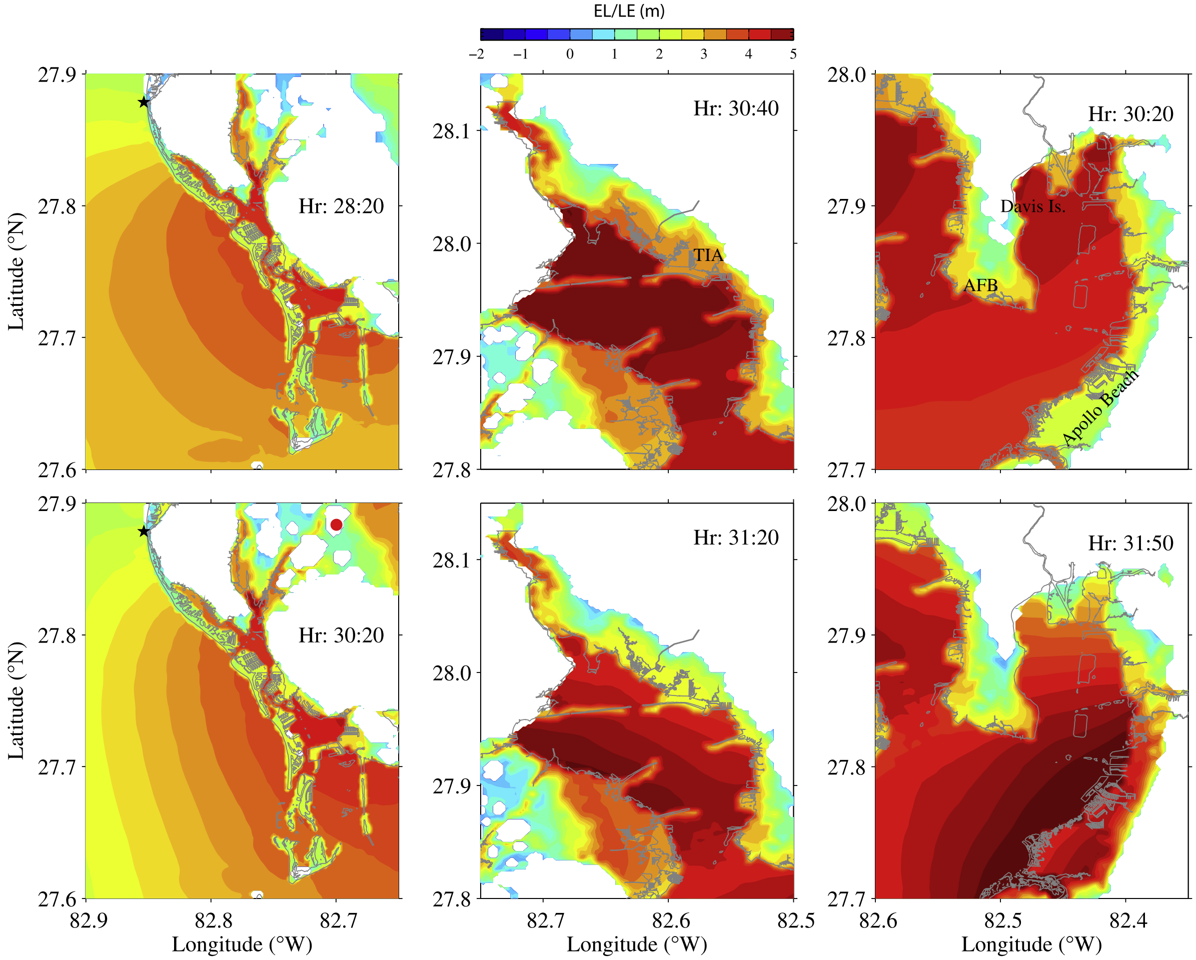

Figure 6. Planar views of the model-simulated maximum surge relative to the local land elevations (EL/LE) at subdomains emphasizing St. Pete Beach (left panels), Old Tampa Bay (middle panels), and Hillsborough Bay (right panels). The respective times for maximum surge are provided.

landfall amounts still occurs. In other words a direct hit is not necessary for substantive damage to occur by hurricane storm surge.

[27] Interestingly, despite the wind speed at EK being larger than at SPB around landfall time for just about any of these experiments, the surge at SPB actually exceeds that at EK (consider the TS and IRB landfall plots, for instance). This is a consequence of local geometry. SPB is a long, continuous barrier island, whereas EK, at the bay mouth, is surrounded by water so water must accumulate at the former, whereas it can flow past the latter. Such observation heightens the need of high horizontal resolution to enable a model to accurately portray inlets, waterways, and bayous.

[28] We are fortunate not to have observations from Tampa Bay to validate these simulations. However, we can draw some useful comparisons to the storm surge produced by Hurricane Ivan in the Pensacola Bay vicinity. Both the actual Pensacola Bay situation and the IRB landfall simulation for Tampa Bay had the storm center located nearly the same distance from the bay mouth (~55 km for Pensacola Bay and ~50 km for Tampa Bay). The maximum surges observed at Pensacola Beach and the upper reaches of Pensacola Bay were 3.6 m and 4.5 m, respectively. The comparative numbers for the Ivan-like IRB landfall surges at the SPB barrier islands and the upper reaches of Tampa Bay are ~5 m and ~6.5 m, respectively. Higher surges found near the Tampa Bay coastline than at the Pensacola Bay coastline are explained on the basis of the broader continental shelf offshore of Tampa Bay. Within the bay, the surge difference between upstream end and bay mouth can be crudely estimated as $\Delta\zeta = L\cdot(\tau_s - \tau_b)/gh$, where L is the length from bay mouth to its head and h is the bay mean depth. Assuming the same surface and bottom stresses and using h_1 = 3.5 m, L_1 = 30 km for Pensacola Bay and h_2 = 4 m, L_2 = 55 km for Tampa Bay, we estimate $\Delta\zeta_1 \approx 1$ m for Pensacola Bay and $\Delta\zeta_2 \approx 1.6$ m for Tampa Bay, consistent with our simulation results. This at least provides a consistency check on the Tampa Bay simulation using Ivan-like meteorological forcing.

4. Dynamics Analysis

[29] Whereas the balance tendency between the vertically integrated pressure gradient force and the difference between the surface and bottom stresses that underlies hurricane storm surge is well known, it is recognized that accelerations and horizontal friction may also be important in geometrically complex, shallow estuaries. Thus we examine

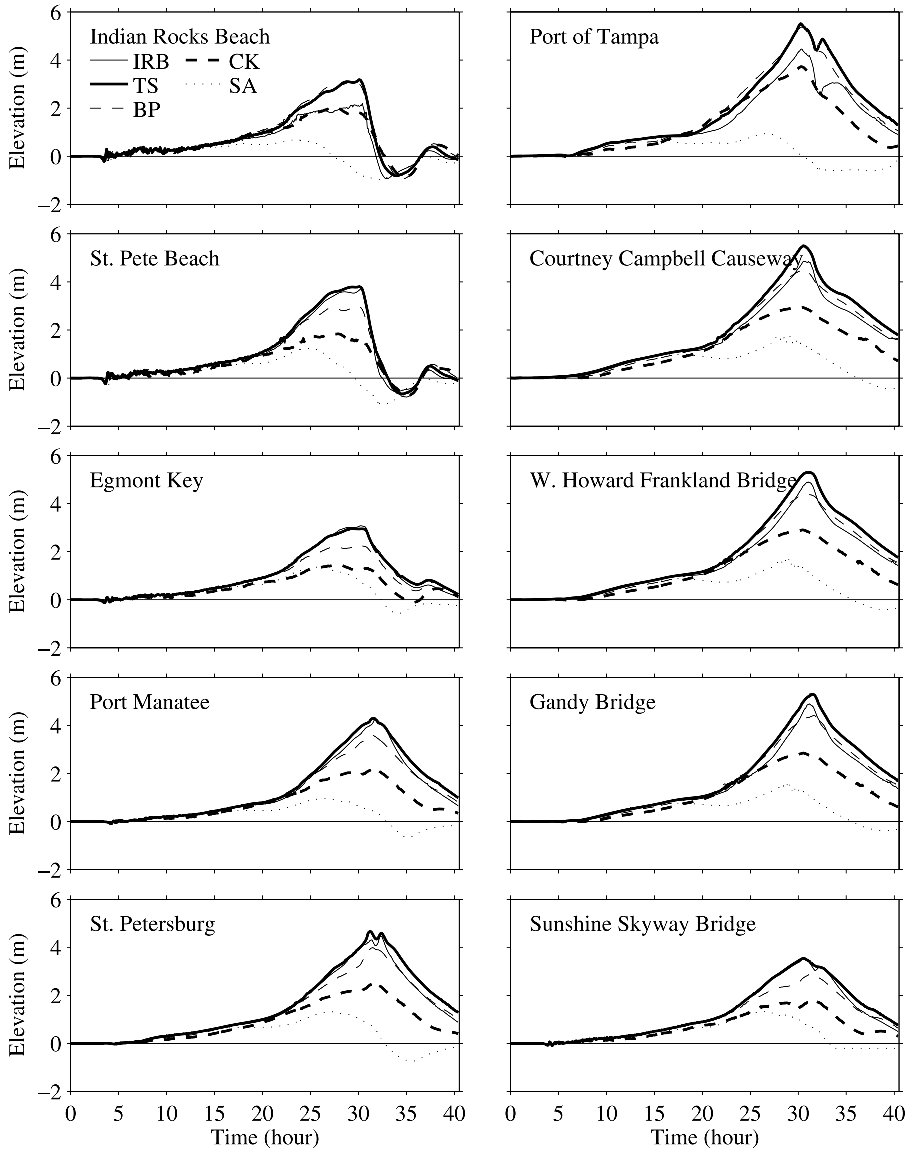

Figure 7. Time series of the model-simulated surge sampled at (counterclockwise from the top left): Indian Rocks Beach, St. Pete Beach, Egmont Key, Port Manatee, St. Petersburg, the Port of Tampa, the Courtney Campbell Causeway, the Howard Frankland Bridge, the Gandy Bridge, and the Sunshine Skyway Bridge. The thin solid lines are for the IRB landfall; the bold solid lines are for the TS landfall; the thin dashed lines are for the BP landfall; the bold dashed lines are for the CK landfall; and the dotted lines are for the SA landfall.

the nonlinear dynamics of the storm surge simulation for Tampa Bay based on the vertically integrated momentum equations:

$$\underbrace{-gH\nabla\zeta}_{(I)} + \underbrace{\frac{\vec{\tau}_s}{\rho_0}}_{(II)} - \underbrace{\frac{\vec{\tau}_b}{\rho_0}}_{(III)} = \underbrace{\vec{R}}_{(IV)} \tag{11}$$

where the gradient operator, $\nabla = \vec{i}\frac{\partial}{\partial x} + \vec{j}\frac{\partial}{\partial y}$; ζ is the sea level; $H = h + \zeta$ is the total water depth; $\vec{\tau}_s$ and $\vec{\tau}_b$ are the surface wind stress and the bottom friction stress, respectively; and $\vec{R}$ (hereafter referred to as the residual term) is the sum of the local and Coriolis accelerations, the advective accelerations, and the horizontal diffusion, each calculated separately before summation. Of these, we note that the horizontal diffusion is small such that $\vec{R}$ can be considered as the total acceleration: the material acceleration, plus the Coriolis acceleration.

[30] Equation (11) may be diagnosed separately for 2-D and 3-D simulations so whereas the results provided in section 3 are for a fully 3-D simulation here we will concern ourselves with the differences that can arise from these different model formulations. Of particular concern is with the bottom friction parameterization. A 3-D model uses equations (8) and (9) in a kinematically and dynamically consistent manner in so far as the logarithmic bottom boundary layer is addressed via a near-bottom velocity and a boundary layer scaled drag coefficient. A 2-D model, on the other hand, is limited to using a vertically averaged velocity, which may not necessarily be indicative of

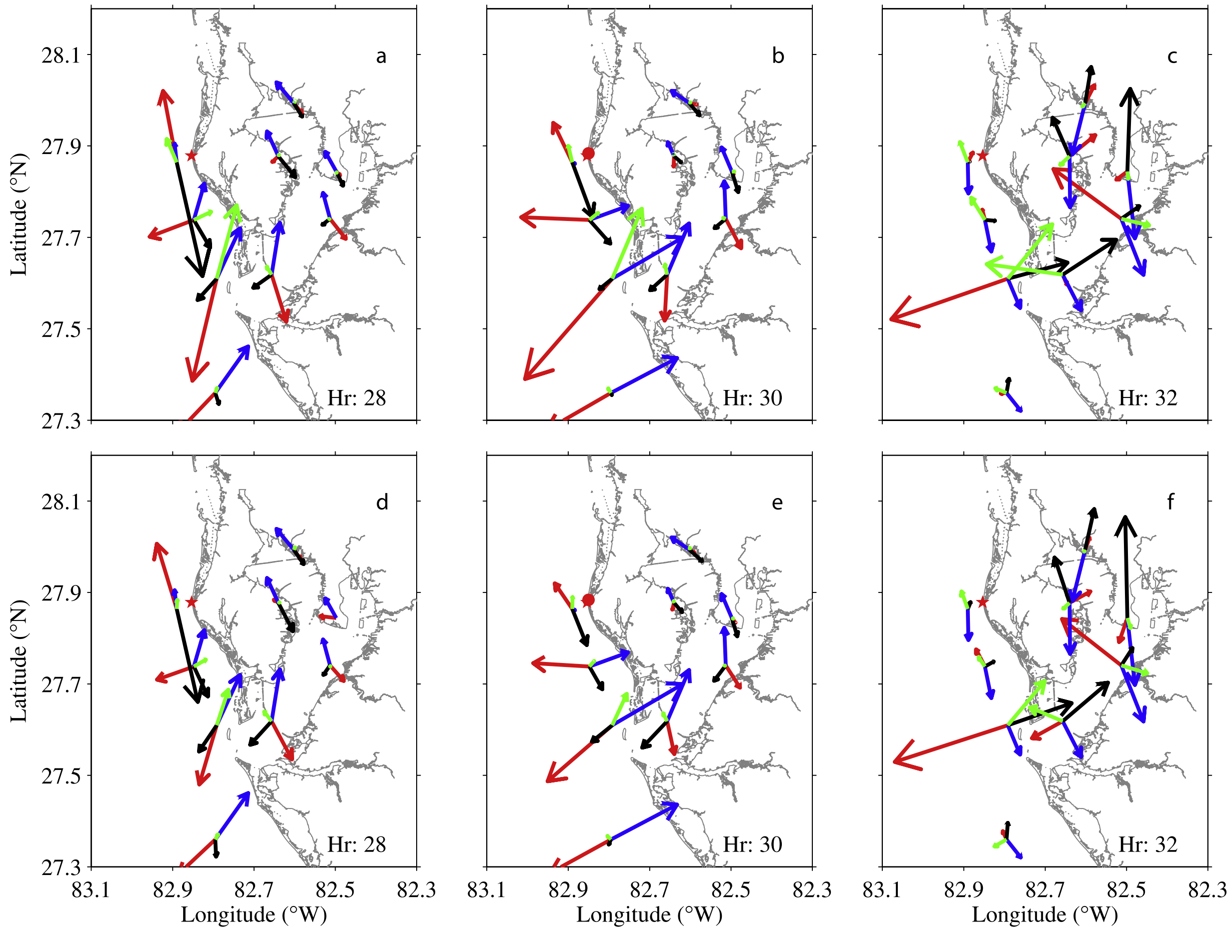

Figure 8. Planar views of the vectors comprising the momentum balances for the (a–c) 3-D and the (d–f) 2-D simulations at hours 28, 30, and 32. Red denotes the pressure gradient; blue denotes the wind stress; black denotes the bottom stress; and green denotes the residual accelerations as defined by equation (11). The asterisk denotes the IRB landfall location, and the solid red circle denotes the storm center location.

the near-bottom velocity. If the bottom stress estimated by a 2-D model is inconsistent with the bottom stress estimated with a 3-D model then aside from the residual term the only other recourse in the momentum balance is for the pressure gradient force (and hence the surface slope) to be altered. Since surge is the temporal and spatial integral of the surface slope, errors in bottom stress will result in errors in surge. We explore this by comparing results from 3-D and 2-D simulations; in particular, the dynamical balances, the horizontal velocity vectors that go into the bottom stress parameterizations, and the resulting differences in surge heights.

[31] First consider the vertically integrated dynamical balances. The terms in equation (11) all vary in time and space throughout the storm surge evolution. Sampled over a coarse grid chosen to be representative of the various depth regimes in the Tampa Bay area, Figures 8a, 8b, and 8c provide snapshots of the vectorial balances for the 3-D, IRB landfall simulation case at: (1) hour 28, when the storm center was still offshore; (2) hour 30, the time of IRB landfall; and (3) hour 32, when the storm was east of Tampa Bay. Unlike an idealized steady state balance for a straight channel in which all vectors would be collinear, with the pressure gradient term being the difference between the two stress terms, we see a much more complex evolution. Since the pressure gradient term must balance the sum of all of the other terms, any errors in these other terms will be reflected in the pressure gradient force and hence in the storm surge.

[32] Errors may arise in several ways. Assuming a perfect model, with perfect wind and pressure fields, we see that the starting point for error is with the wind stress parameterization (equations (6) and (7)). Here C_d increases with wind speed, but only up to a maximum value of 2.11×10^{-3} at a wind speed of 25 ms^{-1}, beyond which C_d is constant. Other model parameterizations allow C_d to increase further with increasing wind speed. The surface wind stress parameterization may also incur error to the extent that the relative wind speed is in error. Next comes errors in bottom stress, by virtue of incorrect near-bottom speed or drag coefficient, followed by non-linear effects. These errors will combine vectorially to produce a pressure gradient error.

[33] Our main concern here is with errors that may follow from the model construct itself, and in particular the difference between 3-D and 2-D models. To compare these different model constructs with consistent dynamics, we approximated a 2-D model by using three sigma levels instead of 11 (as in the 3-D case). By distributing the three

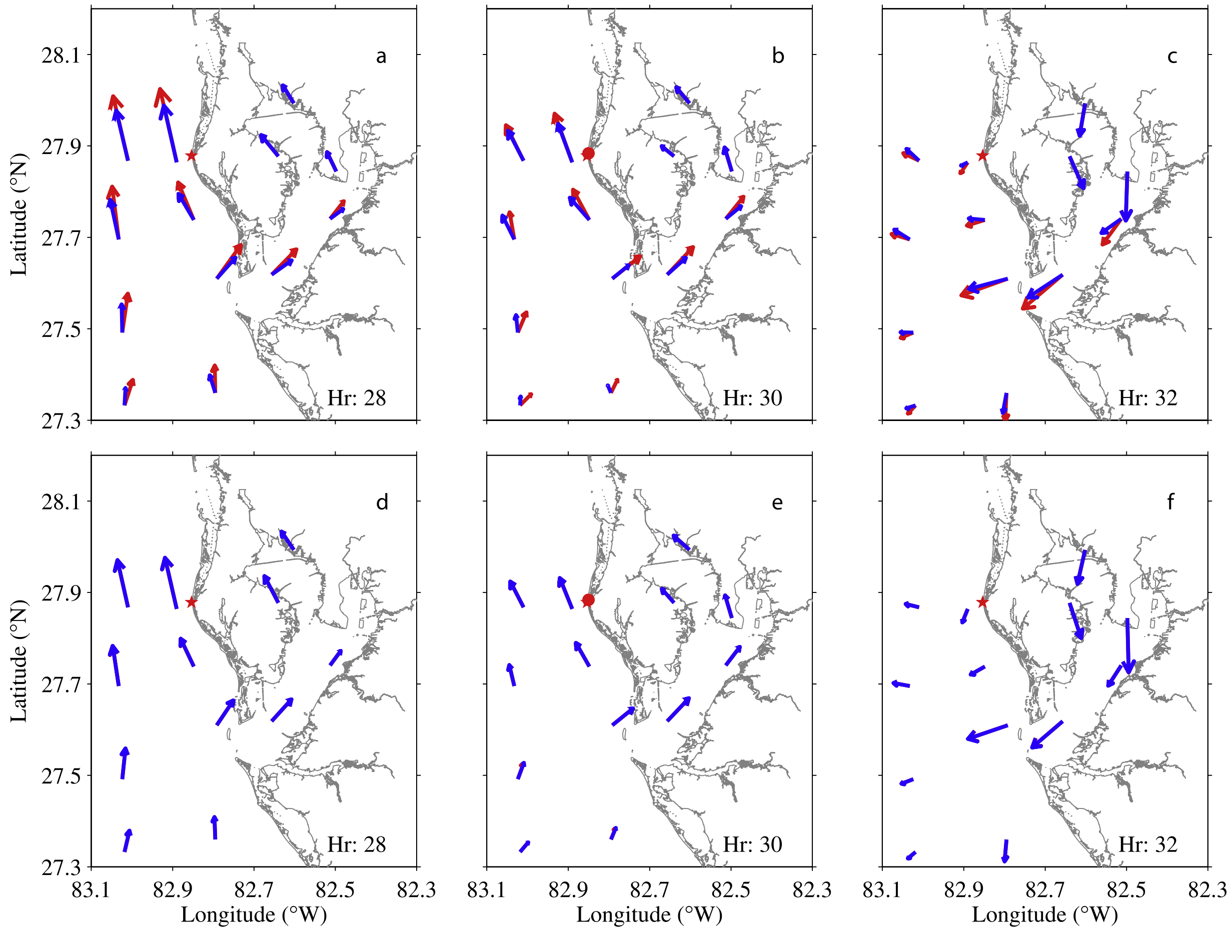

Figure 9. Planar views of the model-simulated vertically averaged velocity (red) and near-bottom velocity (blue) vectors for the (a–c) 3-D and the (d–f) 2-D simulations at hours 28, 30, and 32. The asterisk denotes the IRB landfall location, and the solid red circle denotes the storm center location.

sigma levels at the surface ($\sigma = 0$), the bottom ($\sigma = -1$) and near the bottom ($\sigma = -0.9$), we maintain the same drag coefficient formulation and hence the same C_z as in the 3-D case. As a computational expediency we use the upper sigma layer velocity for the 2-D bottom stress determination, and we will show that this does not cause any additional error. Figures 8d, 8e, and 8f provide snapshots of the vectorial balances for the 2-D, IRB landfall simulation case that can be compared directly with their 3-D counterparts in Figures 8a, 8b, and 8c.

[34] The differences between these 3-D and 2-D momentum balances are subtle, but important. The reader can consider each location and time separately. Here for orientation purposes we will point out a few obvious examples. Consider the location just outside the bay to the west of Egmont Key. The directions of the four vectors comprising the balances for 3-D and 2-D are nearly the same at hour 28 except that the bottom stress vector is smaller and the residual (which is mostly acceleration) is larger for the 3-D case, which causes the pressure gradient vector to be much larger for the 3-D than for the 2-D case. The same can be said of hour 30. These differences are less pronounced at hour 32. Next, consider the location just inside the bay to the east of Egmont Key. The balances for 3-D and 2-D are nearly the same at hour 28 except that the bottom stress vector is smaller for the 3-D case so that the residual and the pressure gradient vectors must adjust accordingly. The same can be said of hour 30, but now the adjustments are larger and both the magnitude and direction of the pressure gradient vectors are now noticeably different. These differences become more palpable at hour 32, when the pressure gradient points in an entirely different direction and the residual is therefore larger than any of the other individual vectors. Similarly, consider the vectors farther up the bay and just to the west of Apollo Beach. At hours 28 and 30 the 3-D and 2-D cases are close to one another, but at hour 32 the 3-D pressure gradient vector is larger than the 2-D pressure gradient vector, and the residuals must adjust accordingly.

[35] The explanations for these dynamical balance differences follow from the differences between the vertically averaged versus the vertically dependent velocities. Figures 9a, 9b, and 9c show these for the 3-D, IRB landfall simulation case at hours 28, 30, and 32, and Figures 9d, 9e, and 9f provide the counterparts for the 2-D case. No differences are seen for the 2-D case since the near-bottom (between $\sigma = -0.9$ and $\sigma = -1$) and the depth-averaged velocities are nearly identical. However, the differences for the 3-D case are quite evident. These differences translate into bottom stress differences and hence vertically averaged momentum balance differences. A

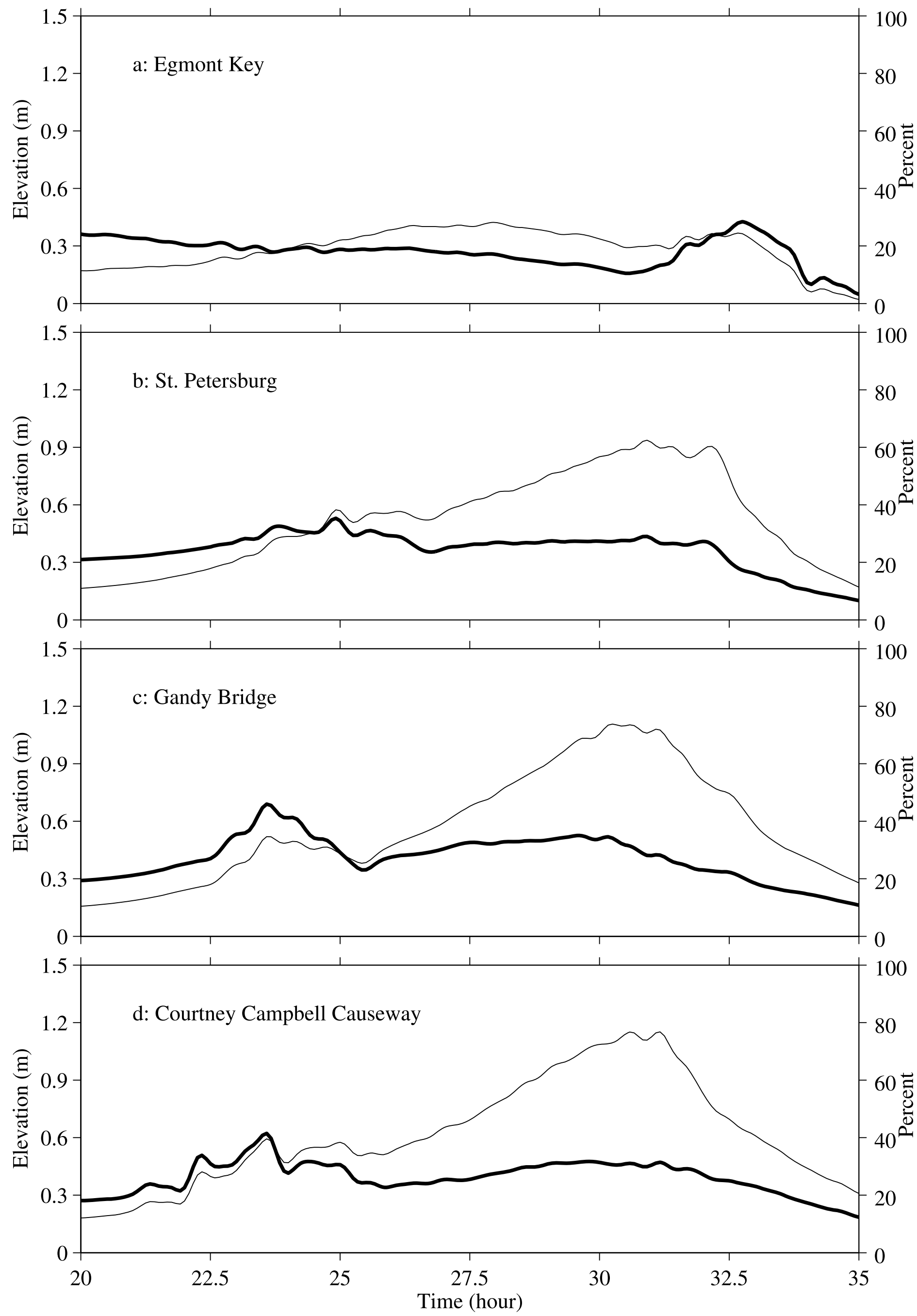

Figure 10. Time series of the absolute differences between surge heights simulated using 3-D and 2-D model constructs (thin lines) and their percentage differences (bold lines) sampled at (a) Egmont Key, (b) St. Petersburg, (c) the Gandy Bridge, and (d) the Courtney Campbell Causeway.

secondary effect is that the non-linear acceleration terms also vary with depth so their vertical averages will be different to the extent that the velocity vectors are depth-dependent. Hence significant dynamical balance differences occur between models constructed using 3-D, versus 2-D formulations.

[36] How these dynamical balance differences translate to storm surge differences is illustrated by Figure 10. With the bottom stress generally overestimated in the 2-D case, the pressure gradient force tends to be underestimated. Hence the storm surge heights are also underestimated by the 2-D model relative to the 3-D model. Focusing on positions going up the bay from the mouth to the head: (1) Egmont Key at the bay mouth; (2) St. Petersburg, mid-way up the bay; (3) Gandy Bridge, near the mouth of Old Tampa Bay; and (4) Courtney Campbell Causeway, near the head of Old Tampa Bay, Figure 10 shows time series of both the absolute differences between surge heights under 3-D and 2-D formulations and their percent differences. The surge height differences are seen to increase with increasing distance up the bay along with the surge heights. At the bay mouth the difference is about 0.5 m and this increases to about 1.2 m at the Courtney Campbell Causeway. The

corresponding percent differences (at the peak of the storm surge) range between 25%–35%. Such storm surge modeling errors, simply on the basis of 3-D versus 2-D model constructions, are hardly insignificant.

5. Discussion

[37] Are these findings really new, and why should we be concerned? Differences between bottom stress calculated using 2-D and 3-D models have been considered before. For instance, *Grenier et al.* [1995] compared 2-D and 3-D tidal harmonics simulations for a shallow embayment, and varied the magnitude of the (constant) bottom drag coefficient to best calibrate the models. After calibration, their 2-D and 3-D simulation results were similar for the astronomical tidal constituents, whereas their 2-D results were better for the overtides. Previously, *Davies* [1988] had compared storm surge simulations using 2-D and 3-D models. By introducing a modified bottom stress for the 2-D model, they arrived at results similar to their 3-D case. Without a modified bottom stress the 2-D model underestimated the surge height of the 3-D model, consistent with our results.

[38] Such studies have not garnered much attention, however, nor are we aware of the dynamical balances that give rise to these differences having been diagnosed for storm surge. One reason may be because the purview of hurricane storm surge modeling in the U.S. has been with NOAA, USACE, and FEMA. Hurricane storm surge modeling has therefore been viewed as a task sufficiently accomplished as to be considered operational. Moreover, the hindcast analyses for the coastal inundation by Hurricane Katrina, as recently performed by the USACE Intergovernmental Performance Evaluation Taskforce (IPET), provide excellent results when gauged quantitatively against available data [see https://ipet.wes.army.mil/ and Westerink et al., submitted manuscript, 2008]. The IPET used a very high resolution version of ADCIRC [e.g., *Westerink and Luettich*, 1991], driven by post-storm analyzed winds and pressure fields, and also coupled to a wave model. These IPET analyses are the state-of-the-art, and the errors are impressively small. However, the errors derive from a calibrated hindcast so they beg the question: how might the ADCIRC 2-D formulation have impacted the hindcast relative to a 3-D formulation?

[39] To answer this question we must consider both the surface and bottom stress parameterizations used by ADCIRC. From the IPET report, wind stress is computed by:

$$\vec{\tau}_{\mathrm{s}} = \mathrm{C_d}\rho_{\mathrm{a}}|\vec{\mathrm{V}}_{\mathrm{w}}|\vec{\mathrm{V}}_{\mathrm{w}}, \tag{12}$$

where ρ_a is air density, $\vec{V}_w$ is wind speed at 10 m height, and C_d, the drag coefficient dependent on wind speed, is given by formula of *Garratt* [1977]:

$$\mathrm{C_d} = \left(0.75 + 0.067|\vec{\mathrm{V}}_{\mathrm{w}}|\right) \times 10^{-3} \tag{13}$$

without an upper bound. Bottom stress is determined by:

$$\vec{\tau}_{\mathrm{b}} = C_f \rho_{\mathrm{w}}|\vec{\mathrm{V}}_{\mathrm{b}}|\vec{\mathrm{V}}_{\mathrm{b}}, \tag{14}$$

where ρ_w is water density, $\vec{V}_b$ is depth-averaged water velocity, and C_f is the bottom friction coefficient, which is a function of water depth, i.e.

$$\mathrm{C_f} = C_{f\,\mathrm{min}}\left[1 + \left(\frac{H_b}{H}\right)^{\theta}\right]^{\frac{\gamma}{\theta}} \tag{15}$$

where H_b is defined as the break depth, beyond which C_f takes on a minimum value $C_{f\mathrm{min}}$, and γ and θ are two parameters that determine the variation of C_f with depth. For the IPET application of ADCIRC to the Hurricane Katrina storm surge simulation, H_b = 2 m, $C_{f\mathrm{min}}$ = 0.003, θ = 10, and γ = 4/3.

[40] Two fundamental issues are identified. First, the surface stress parameterization for ADCIRC by the IPET allows the drag coefficient, C_d, to increase unboundedly with increasing wind speed. Second, the same vertically averaged, versus vertically dependent velocity problem as explained in the previous section applies to ADCIRC. Combined, we see that increased surface stress can compensate for increased bottom stress, allowing the calibrated model result to match the observations for reasons that may or may not be correct. For instance, had we used the IPET ADCIRC surface stress parameterization in our simulation for an Ivan-like hurricane, then the C_d would have been about twice as large as the C_d obtained with equation (7) for a 50 ms^{-1} wind, and the surge heights would therefore have been proportionately larger than those shown in Figures 5–7. For the bottom stress parameterization we did employ values of C_z comparable to those of the IPET ADCIRC. By placing an upper limit on the magnitude of C_z at 0.005, we are close to the IPET depth-dependent values, which, for example, are 0.003 and 0.007 for depths of 2 m and 1 m, respectively. (As an aside, we did test the sensitivity of our model calculations to the assignment of a C_z upper limit. Both the 3-D and the 2-D results were found to change proportionately, with their absolute differences being about the same.) The IPET values increase for decreasing depth so if anything the bottom stress values for IPET are larger than the bottom stress values used herein, both on the basis of C_f and near-bottom velocity overestimation. Thus while the Hurricane Katrina IPET results with the 2-D ADCIRC are truly remarkable in their quantitative agreement with available data, are they remarkable for the correct reason?

[41] This is an important question since ADCIRC in its 2-D formulation is being used to provide guidance for rebuilding the city of New Orleans and for updating flood insurance rate maps for the coastal United States. Similarly, local emergency management agencies derive their guidance from the 2-D simulations made using the NOAA SLOSH model [e.g., *Jelesnianski et al.*, 1992]. Whereas calibration data (and the inclusion of a coupled wave model) rendered the IPET simulations to be highly accurate, hypothetical rate map and forecast studies may not have calibration data to rely on. For these applications we require models that are complete-enough in their dynamics and parameterizations, are supported well-enough by bathymetry and elevation data, and are driven by sufficiently accurate forcing functions. The next question is how well do we know the parameterizations?

[42] Reviews on the momentum exchanges for low wind speeds and for hurricanes are provided by *Edson et al.* [2007] and *Black et al.* [2007], respectively. *Powell et al.* [2003] focus on the structure of the wind profile under the high wind conditions associated with tropical storms and provides estimates on friction velocity, surface roughness, and C_d on the basis of these observed wind profiles. The suggestion is that C_d may reach a maximum value at wind speeds less than 30 ms^{-1} and that C_d may actually decrease at higher wind speeds owing to a slip layer induced by bubbles and foam. The implied maxima in C_d are roughly between $2.0-2.5 \times 10^{-3}$, which is of the range employed here, and about a factor of two less than employed in the IPET, Hurricane Katrina storm surge simulations. More recent studies by *Donelan et al.* [2004] and *Moon et al.* [2007] support these suggestions on drag coefficient limitation at high wind speeds. Bottom stress parameterizations may be even more difficult to quantify since roughness depends on bottom type and resuspension of sediments. Regardless of the variation in C_f, the velocity used in the bottom stress parameterization will still be relevant, and for that the concern points to vertically averaged, versus vertically dependent velocity, which will differ in all but the shallowest depths.

6. Summary and Conclusions

[43] The finite volume coastal ocean model of *Chen et al.* [2003] was used to investigate the coastal inundation potential by hurricane storm surge for the Tampa Bay, FL region. In view of the fact that this region has not experienced a direct hit by a major hurricane since 1921, we used the wind and pressure fields estimated for Hurricane Ivan (which made landfall on the Florida/Alabama border in summer 2004) by stretching and rotating the actual Ivan track to point eastward toward the west coast of Florida and then rotating the wind and pressure fields relative to the new track. The responses to such hurricanes with tracks making landfall at various locations from Sarasota, in the south, to Cedar Keys, in the north, were investigated. Along with descriptions of inundation responses, we explored the dynamical balances that comprise hurricane storm surge and, in particular, the differences that arise between 3-D, versus 2-D model simulations.

[44] Two conclusions are drawn, one of local importance, the other of more general importance. Of local importance is the realization that the Tampa Bay, FL region, by virtue of a broad shelf width, an elongate and geometrically complex embayment, and low land elevations, is vulnerable to inundation by hurricane storm surge. Moreover, the potential for disaster is as serious as occurred along the Mississippi coastline during Hurricane Katrina.

[45] Of a more general concern is the finding that substantive differences exist in the estimation of hurricane storm surge when using 3-D, versus 2-D model constructs. The explanation is straight-forward, deriving from the differences between the bottom stresses associated with vertically dependent, versus vertically averaged velocities. By overestimating bottom stress, a 2-D model underestimates surge height. While this may not be problematic in a hindcast, owing to the availability of data for calibration (as evidenced by the IPET, Hurricane Katrina analyses), forecasts or other advisories without the benefit of calibration data may be in significant error. Presently, the U.S. agencies charged with hurricane protection planning, advisories, and flood insurance rate map generation employ 2-D model constructs for their hurricane storm surge simulations. Regardless of the model itself, our findings suggest that the model constructs be changed to 3-D. Moreover, it seems clear from the extant literature that additional studies are necessary to improve upon the parameters that are used for calculating both the surface and the bottom stresses.

[46] **Acknowledgments.** Support was by the Office of Naval Research grants N00014-05-1-0483 and N00014-02-1-0972 and by the National Oceanic and Atmospheric Administration grant NA07NOS4730211. The second of these is for the Southeast Atlantic Coastal Ocean Observing System (SEACOOS). and the third is related to the Southeast Atlantic Coastal Ocean Observing Regional Association (SECOORA). Changsheng Chen, University of Massachusetts, Dartmouth, kindly provided the FVCOM code along with helpful discussions.

References

Black, P. G., E. A. D'Asaro, W. M. Drennan, J. R. French, P. P. Niller, T. B. Sanford, E. J. Terrill, E. J. Walsh, and J. A. Zhang (2007), Air-Sea exchange in hurricanes, *Bull. Am. Meteorol. Soc.*, *88*, 357–374.

Blumberg, A. F., and G. L. Mellor (1987), A description of a three-dimensional coastal ocean circulation model, in *Three-dimensional Coastal Ocean Models*, *Coastal and Estuarine Series*, vol. 4, edited by N. Heaps, pp. 1–16, AGU, Washington, D. C.

Chen, C. S., H. D. Liu, and R. C. Beardsley (2003), An unstructured, finite-volume, three-dimensional, primitive equation ocean model: Application to coastal ocean and estuaries, *J. Atmos. Ocean. Technol.*, *20*, 159–186.

Chen, C. S., J. H. Qi, C. Y. Li, R. C. Beardsley, H. C. Lin, R. Walker, and K. Gates (2008), Complexity of the flooding/drying process in an estuarine tidal-creek salt-marsh system: An application of FVCOM, *J. Geophys. Res.*, *113*, C07052, doi:10.1029/2007JC004328.

Davies, A. M. (1988), On formulating two-dimensional vertically integrated hydrodynamic numerical models with an enhanced representation of bed stress, *J. Geophys. Res.*, *93*, 1241–1263.

Donelan, M. A., B. K. Haus, N. Reul, W. J. Plant, M. Stiassnie, H. C. Graber, O. B. Brown, and E. S. Salzman (2004), On the limiting aerodynamic roughness of the ocean in very strong winds, *Geophys. Res. Lett.*, *31*, L18306, doi:10.1029/2004GL019460.

Edson, J. E., et al. (2007), The coupled boundary layers and air-sea transfer experiment in low winds, *Bull. Am. Meteorol. Soc.*, *88*, 341–356.

Galperin, B., L. H. Kantha, S. Hassid, and A. Rosati (1988), A quasi-equilibrium turbulent energy model for geophysical flows, *J. Atmos. Sci.*, *45*, 55–62.

Garratt, J. R. (1977), Review of drag coefficients over oceans and continents, *Mon. Weather Rev.*, *105*, 915–929.

Grenier, R. R., R. A. Luettich, and J. J. Westerink (1995), A comparison of the nonlinear frictional characteristics of two-dimensional and three-dimensional models of a shallow tidal embayment, *J. Geophys. Res.*, *100*, 13,719–13,735.

Hagy, J. D., J. C. Lehrter, and M. C. Murrell (2006), Effects of hurricane Ivan on water quality in Pensacola Bay, Florida, *Estuaries Coasts*, *29*, 919–925.

Hess, K. (2001), Generation of tidal datum fields for Tampa Bay and the New York Bight, in *NOAA Tech. Rep. NOS CS 11*, 43 pp., National Ocean Service, NOAA, Silver Spring, Md.

Holland, G. J. (1980), An analytic model of the wind and pressure profiles in hurricanes, *Mon. Weather Rev.*, *108*, 212–1218.

Hubbert, G. D., and K. L. McInnes (1999), A storm surge inundation model for coastal planning and impact studies, *J. Coastal Res.*, *15*, 168–185.

Jelesnianski, C. P., J. Chen, and W. A. Shaffer (1992), SLOSH: Sea, lake, and overland surges from hurricanes, *NOAA Tech. Report NWS 48*, 77 pp., National Weather Service, NOAA, Silver Spring, Md.

Large, W. G., and S. Pond (1981), Open ocean momentum fluxes in moderate to strong winds, *J. Phys. Oceanogr.*, *11*, 324–336.

Mellor, G. L., and T. Yamada (1982), Development of a turbulence closure model for geophysical fluid problems, *Rev. Geophys.*, *20*, 851–875.

Moon, I.-J., I. Ginnis, T. Hara, and B. Thomas (2007), A physics-based parameterization of air-sea momentum flux at high wind speeds and its impact on hurricane intensity predictions, *Mon. Weather Rev.*, *135*, 2869–2878.

Peng, M. C., L. Xie, and L. J. Pietrafesa (2006), A numerical study on hurricane-induced storm surge and inundation in Charleston Harbor, South Carolina, *J. Geophys. Res.*, *111*, C08017, doi:10.1029/2004JC002755.

Powell, M. D., P. J. Vickery, and T. A. Reinhold (2003), Reduced drag coefficient for high wind speeds in tropical cyclones, *Nature*, *422*, 279–283.

Sallenger, A. H., H. F. Stockdon, L. Fauver, M. Hansen, D. Thompson, C. W. Wright, and J. Lillycrop (2006), Hurricane 2004: An overview of their characteristics and coastal change, *Estuaries Coasts*, *29*, 880–888.

Signorini, S. R., J. S. Wei, and C. D. Miller (1992), Hurricane-induced surge and currents on the Texas-Louisiana shelf, *J. Geophys. Res.*, *97*, 2229–2242.

Smagorinsky, J. (1963), General circulation experiments with the primitive equations. I: The basic experiment, *Mon. Weather Rev.*, *91*, 99–164.

Wang, D. W., D. A. Mitchell, W. J. Teague, E. Jarosz, and M. S. Hulbert (2005), Extreme waves under hurricane Ivan, *Science*, *309*, 896.

Weisberg, R. H., and L. Zheng (2006a), Circulation of Tampa Bay driven by buoyancy, tides, and winds, as simulated using a finite volume coastal ocean model, *J. Geophys. Res.*, *111*, C01005, doi:10.1029/2005JC003067.

Weisberg, R. H., and L. Zheng (2006b), Hurricane storm surge simulations for Tampa Bay, *Estuaries Coasts*, *29*, 899–913.

Weisberg, R. H., and L. Zheng (2006c), A simulation of the hurricane Charley storm surge and its breach of North Captiva Island, *Fla. Sci.*, *69*, 152–165.

Weisberg, R. H., R. He, Y. Liu, and J. I. Virmani (2005), West Florida shelf circulation on synoptic, seasonal, and inter-annual time scales, in *Circulation in the Gulf of Mexico: Observations and Models*, *Geophys. Monogr. Ser.*, vol. 161, pp. 325–347, AGU, Washington, D. C.

Westerink, J. J., and R. A. Luettich (1991), Tide and storm surge prediction in the Gulf of Mexico using model ADCIRC-2D, Report to U. S. Army Engineers Waterways Experiment Station, Vicksburg, Miss., 112 pp., July.

R. H. Weisberg and L. Zheng, College of Marine Science, University of South Florida, 140 Seventh Avenue South, St. Petersburg, FL 33701-5016, USA. (weisberg@marine.usf.edu)